ELSEVIER

Polymer 41 (2000) 3357–3364

polymer

# Investigation of molecular orientation in melt-spun high acrylonitrile fibers

J.A. Davidson[a], H.-T. Jung[a,1], S.D. Hudson[a,*], S. Percec[b]

[a]*Department of Macromolecular Science and Engineering, Case Western Reserve University, 10900 Euclid Avenue, Cleveland, OH 44106-7202, USA*
[b]*BP Amoco Chemicals, Cleveland, OH, USA*

Received 14 May 1999; received in revised form 27 July 1999; accepted 29 July 1999

**Abstract**

The orientation and crystal size of a series of melt-spun high acrylonitrile AMLON® and solution-spun commercial acrylic fibers are investigated by optical and X-ray diffraction analysis. The effect of different processing steps is examined. The image intensity of a birefringent fiber under cross polarizers is fitted accurately, assuming that the birefringence across the entire fiber cross-section is uniform. The molecular orientational order parameter of the fiber, as measured by X-ray diffraction, correlates linearly with its birefringence. The orientation of the melt-spun fibers is as good or better than that of commercial solution-spun fibers, and it increases dramatically in the melt-spun fibers when they are post drawn or spun from higher molecular weight resins. Orientation is affected only slightly by annealing processes, which in turn increase the crystal size in the fiber. 

*Keywords*: Molecular orientation; Melt-spun high acrylonitrile fibers; Optical and X-ray diffraction analysis

## 1. Introduction

Acrylonitrile polymerizes by a free radical mechanism and the resulting polymer (PAN) is mostly atactic [1]. However, some degree of order is present in the polymer due to the large magnitude of the dipole moment of the nitrile groups. This leads to strong intrachain and interchain interactions through secondary bonding. Upon heating, the adjacent nitrile groups on the polymer chains cyclize to form six-membered rings, and PAN undergoes a degradation reaction prior to melting at 320–330°C [2,3]. Only rarely is the homopolymer used for fiber spinning, and virtually all commercial acrylic fibers are spun from acrylonitrile polymers containing 1–15 wt.% comonomer [4]. The spinning processes most commonly used for acrylic fibers involve highly polar solvents, such as *N*,*N*-dimethylformamide (DMF), dimethylacetamide (DMAc) and dimethylsulfoxide (DMSO). Melt processable, high acrylonitrile copolymers are currently under development by BP Amoco Chemicals. For the first time, fibers melt-spun from these copolymers were available for study and their property evaluation could provide valuable insights into both the molecular and morphological organization.

The majority of textile fibers have a morphology that can be described by the classical two-phase model [5–7]. In this model, discrete crystalline domains of the order of several hundred angstroms (Å) are mixed with amorphous domains of similar or smaller size. A high degree of crystallinity and high orientation of the crystalline molecular segments impart high tensile strength and modulus to the fibers. The amorphous phase gives rise to toughness and dyeability. In contrast to the crystalline fraction, a low degree of orientation of the amorphous phase is preferred, in order to minimize shrinkage caused by stress relaxation upon heating the material above its glass transition temperature.

Whether polyacrylonitrile can be described by the classical model is debatable. In the ordered phase, irregularly twisted, yet extended atactic polymer chains are packed hexagonally [8,10]. Owing to the strong interchain interactions noted above, this hexagonal columnar phase behaves as a solid, and it is often referred to as a (two-dimensional, 2D) crystal. However, the nature and even the existence of the amorphous phase is a subject of controversy. As-polymerized and solvent cast materials exhibit an amorphous phase [11–13], but highly oriented fibers do not [8,14]. Apparently, the existence of the amorphous phase depends on the processing conditions [15]. The situation may be even more complicated in the case of copolymers.

* Corresponding author.
*E-mail address:* sdh6@po.cwru.edu (S.D. Hudson).
[1] Present address: Department of Chemical Engineering, University of California, Santa Barbara, CA, USA.

0032-3861/00/$ - see front matter 
PII: S0032-3861(99)00536-4

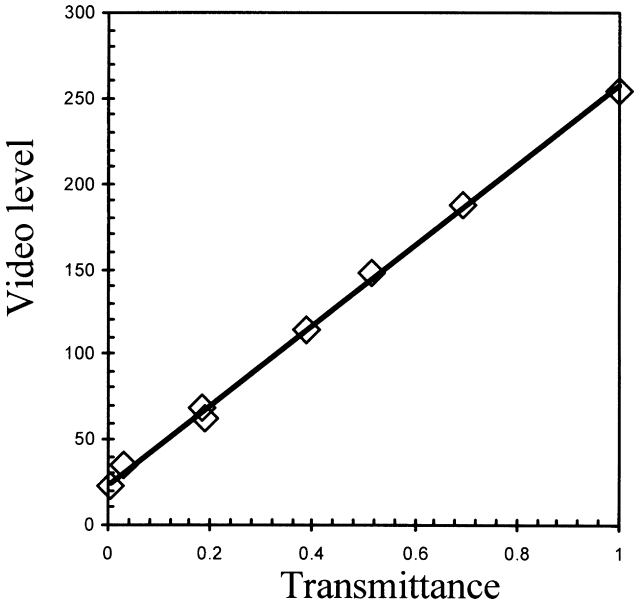


Fig. 1. Calibration of the CCD video signal. The video level is plotted versus light transmission, $T = I/I_0$, as measured by densitometry.

In the typical industrial practice of spinning flexible polymers from the melt state, as-spun fibers are found to have low crystallinity and orientation. Fibers with higher orientation can be obtained by the use of an in-line isothermal bath technique [16–18]. Higher levels of orientation are also achieved as a result of post-drawing processes. In most cases, the drawn fibers are subsequently subjected to annealing by heating and cooling under tension [16–18]. These processes are done continuously as the fiber is passed over heated rollers [19].

Since the molecular orientation in polymer fibers is critical for their performance, several methods to measure orientation have been applied and correlated with one another. Optical birefringence, nuclear magnetic resonance, electron spin resonance, infrared dichroism, polarized Raman spectroscopy and various (mainly X-ray) scattering techniques are among the most popular methods used to characterize different aspects of molecular order. Several of these measurements are related directly to the Hermans orientation function, which is an order parameter based on a second moment of the molecular orientation distribution function [20]. Therefore, the results from different techniques may be compared with each other [17,21]. Each of these techniques has inherent advantages and disadvantages. For example, birefringence is relatively convenient for determining orientation in polymers [22,23]. On the other hand, X-ray scattering analysis of oriented polymers provides an effective means to determine molecular packing, as well as orientation.

The main objective of this investigation is to determine the molecular orientation of new melt-spun, high acrylonitrile polymer fibers using optical and X-ray diffraction methods. In addition, the orientation is examined as a function of spinning conditions and comparisons with commercial fibers spun from solution are made.

## 2. Experimental procedure

Experimental melt-spun high acrylonitrile copolymer fibers (AMLON®) were supplied by BP Amoco Chemicals Inc. These copolymers contained a large fraction of acrylonitrile. The fiber denier was measured from the weight and length of the fiber. For most of the samples, the weight-average molecular weight, as measured by gel permeation chromatography (GPC), was approximately 50,000 g $mol^{-1}$; a few samples having a molecular weight of approximately 90,000 g $mol^{-1}$ were also tested. The thermal transitions of the fibers were measured by DSC, and they indicate a glass transition at approximately 88°C with a broad melting temperature range centered at approximately 225°C. The dynamics of these materials were investigated by rheological analysis, using a Rheometrics RMS 800 mechanical spectrometer. To facilitate this analysis, a copolymer having a slightly higher fraction of comonomer, and therefore a lower melting range (i.e. centered at ~130°C), was used. The linear viscoelastic moduli were measured as a function of frequency and temperature. Based upon the plateau modulus, the molecular weight between entanglements is approximately 5000. Through the time–temperature superposition analysis of measurements taken at lower temperature, the longest relaxation time in the melt at 220°C is approximately 0.01 s for a polymer having a molecular weight of ~50,000. The temperature of the melt during fiber spinning was controlled to within ±2°C. A range of spinning conditions were examined, and the melt temperature was adjusted to temperatures ranging from 220 to 250°C.

Optical measurements were carried out using an Olympus BX-60 microscope equipped with polarizing optics. Compensation was performed with a tilting compensator (Olympus U-CBE) at a wavelength of 546 nm. An interference filter with a narrow transmission at the above mentioned wavelength in conjunction with a quartz halogen light source was employed. Fiber diameter measurements were performed on stored images obtained with a progressive scan CCD camera with 640 × 480 resolution (Costar CV-M10BX) in conjunction with a Graftek™ imaging system. Line profiles were obtained from the video image, and the calibration factor of micron/pixel was determined from the measurement of a certified stage micrometer.

The video intensity level recorded by the CCD camera was calibrated as follows. Clean glass microscope slides were sputter coated with Au/Pd (60/40) for various times ranging from 0 to 8 min, in order to generate films of different optical densities. The optical density was measured using an XRite 310 densitometer, conforming to ANSI standard PH 2.19. After lightly scoring the slides to remove a narrow line of the metal coating, the slides were also

examined with the Olympus microscope, using a 40× pol objective with the numerical aperture equal to 0.7. The condenser numerical aperture was also 0.7. The intensity of the light was kept constant for each slide and was adjusted so that the video reading on the bare glass slide was 255. Stored images were analyzed using a Labview line-profile program. The video level through each of the metal films was then recorded. The response of the CCD camera was determined to be linear (Fig. 1).

To determine the birefringence of a fiber, it was necessary to know both the fiber diameter and the retardation. Of these, the retardation measurement was the most straightforward. Concerning diameter measurement, it can be demonstrated that if the object contrast is generated by light absorption alone, through a thin uniform coating on the fiber, then in the image profile of the object, ideally a square wave, the size information is contained in the period of the fundamental frequency of the Fourier components that compose the image profile [24]. This fundamental period lies very close to the diameter measured at the mean intensity level. In the study cited [24], vertical shadowed metal film replicas were made of the test particles under study to ensure that only light absorption was responsible for contrast. Alternatively, uniformly birefringent fibers may be sized through the application of Eq. (3), as described in the next section.

In the current study, single fibers were mounted flat on a microscope slide by adhesive tape at the ends. A portion of the fiber was covered with a glass slide, while a thin slip of mica was slid underneath the uncovered section. The slide was then placed in a sputter coater (BioRad) and the fiber coated with about 600 Å of Au/Pd (60/40). By removing the mica slip after coating, an absorbing fiber segment could be compared to an uncoated segment (the glass covered portion), and the effect of the refractive index of the mounting media observed. Since the coated fiber section could be considered as an object whose contrast is only due to light absorption, diameter measured on the coated sections was assumed to be the correct diameter if sized by the criteria outlined earlier.

X-ray diffraction patterns were obtained from bundles of parallel fibers on a Philips system using Ni-filtered $CuK_\alpha$ radiation. The fiber specimens were mounted perpendicular to the X-ray beam. Diffraction patterns of fibers were recorded with a flat film camera at room temperature. The specimen to film distance was calibrated from the (111) reflection of $CaF_2$ powder applied to a fiber specimen. The instrumental beam broadening is less than 0.2°, so that a coherence length of at least 400 Å can be measured (see Eq. (1)). Most fibers exhibited only two peaks: the primary $(10\bar{1}0)$ reflection at ~5.3 Å and the weaker, higher order $(11\bar{2}0)$ reflection at ~3.05 Å, both on the equator. (Note: By convention, four Miller indices (*hkil*) are used for identification of planes in hexagonal crystals [25]. The index *i* is sometimes omitted, because it is equal to $-(h + k)$, by definition [25]. For 2D structures, such as those formed by polyacrylonitrile, index *l* equals 0, and may be omitted. Therefore, the planes may be identified using only indices *h* and *k*. The use of these two indices only is common for columnar hexagonal phases and is adopted in this report.)

Through analysis of the shape and intensity of the primary (10) reflection by an Optronics P-1000 digital micro densitometer, the molecular orientation and coherence length of each fiber could be determined. The coherence length ($L$) was determined from the analysis of an equatorial scan using the Scherrer equation:

$$L = 0.9\lambda/(B\cos\theta), \tag{1}$$

where $B$ is the full width (as a function of scattering angle $2\theta$) at half maximum of the (10) reflection. This coherence length is often called the crystal size, because small crystal size is a major contribution to peak broadening, e.g. Ref. [26]. However, lattice distortions and defects within crystals also contribute to peak broadening, e.g. Ref. [26]. In any case, $L$ is a measure of packing perfection. The molecular orientation was calculated from the distribution of intensity as function of azimuthal angle i.e. at a fixed distance from the center of pattern [27]:

$$S = \frac{3}{2}\langle\cos^2\beta\rangle - \frac{1}{2} = \frac{\int I|\sin\beta|(\frac{3}{2}\cos^2\beta - \frac{1}{2})\,\mathrm{d}\beta}{\int I|\sin\beta|\,\mathrm{d}\beta}, \tag{2}$$

where $\beta$ is the azimuthal angle between the axis of a molecular segment and of the fiber and $I$ is the scattering intensity of the (10) reflection at that angle. From the meridional scan, appropriate background corrections were made (see Fig. 3). These corrections were necessary to account for an isotropic fraction of the material, which produces genuine intensity at the same diffraction angle that is independent of azimuth. Otherwise, ignoring this intensity would lead to an overestimation of $S$.

Infrared dichroism was also used to probe the molecular orientation of the fibers. Absorbence spectra were recorded at the same position in the fiber using a linearly polarized IR radiation, with the electric field vector parallel ( $\parallel$ ) and perpendicular ( $\perp$ ) to the fiber axis. Background spectra were recorded under identical conditions. The molecular orientational order parameter, $S$, was determined from the dichroic ratio, $D$, of the nitrile stretching vibration at 2244 $cm^{-1}$, using integrated band intensities between 2270 and 2220 $cm^{-1}$. The calculation was performed using the following equations:

$$D = \frac{A_\parallel}{A_\perp} \tag{3a}$$

$$D_0 = 2\cot^2\alpha \tag{3b}$$

$$S = \frac{3}{2}\langle\cos^2\theta\rangle - \frac{1}{2} \approx \frac{(D-1)(D_0+2)}{(D+2)(D_0-1)} \tag{3c}$$

where $A_\parallel$ and $A_\perp$ are the respective absorbences, $\alpha$ is the

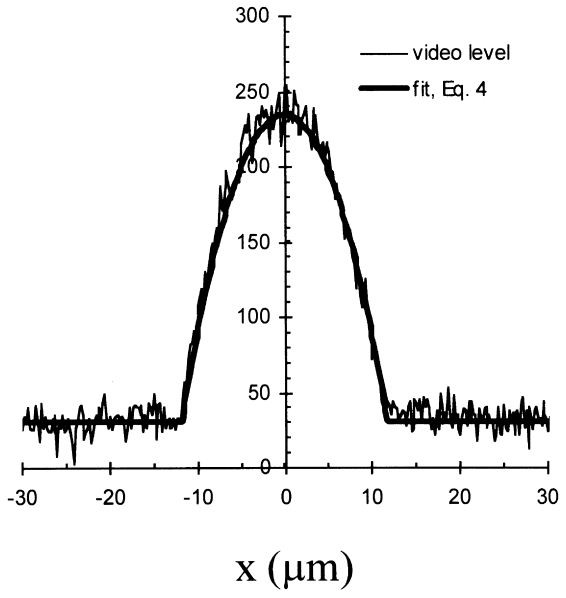


Fig. 2. Measured and predicted intensity profile across an AMLON® fiber (designated **b**) under cross polars.

transition moment angle, and $\theta$ is the angle of the molecular segment relative to the fiber axis [28].

External surface morphology was examined by SEM. After mounting the fibers onto a double-sticky carbon tape, the fibers were sputter coated with ~90 Å gold. To examine the fibers in cross-section, uncoated fibers were embedded inside a capillary filled with epoxy. After curing the epoxy, the capillary was fractured, and the fracture surface was coated as just described. The specimens were examined at 25 keV in a secondary electron imaging mode.

## 3. Results and discussion

The image intensity of a birefringent fiber can be calculated. Here, we assume uniform birefringence across a uniaxially oriented fiber with a circular cross-section. When the principal axes of a birefringent material are oriented 45° with respect to the crossed polarizers, the intensity of transmitted light, wavelength $\lambda$, is given simply by:

$$I = I_0 \sin^2\left(\frac{\pi R}{\lambda}\right), \tag{4}$$

where $R$ is the retardation, which, for a fiber oriented 45° to the polarizer, is the product of the birefringence $\Delta n$ and the path length $t$ through the fiber. The latter is a function of distance $x$ from the central axis of the fiber on a plane perpendicular to the optical axis of the microscope:

$$R = \Delta n t; \qquad t = 2\sqrt{r^2 - x^2}, \tag{5}$$

where $r$ is the fiber radius. Because the fiber is embedded in a non-swelling, near index-matching fluid ([25, $n_D$ = 1.510], Cargille series A was chosen), refraction of the light at the fiber surface is negligible. Agreement between the video gray level and the predicted intensity is excellent (e.g. fiber **b**, Fig. 2), confirming within experimental error, the assumption of uniform birefringence. Because the intensity increases abruptly at the outer edge of the fiber, the diameter of the fiber can also be obtained directly from the image under crossed polars. The diameter measured in this way agrees within experimental error (±0.3 μm) with the diameter measured from the bright field examination of metal-coated fibers, which give simple amplitude modulated images as discussed above. The coated fiber diameter measurement is unchanged by the addition of mounting fluid. However, without mounting fluid, the diameter obtained from the uncoated fiber under crossed polars is approximately 10% larger than that obtained with mounting fluid.

After having measured the fiber diameter and the retardation through the central diameter (i.e. $x = 0$) of the fiber (which represents its maximum retardation), the birefringence of the fiber may be calculated (Eq. (5)). The results for numerous fibers analyzed in this way are presented in Fig. 5.

X-ray diffraction of these copolymer fibers exhibits two equatorial reflections (e.g. fiber **b**, Fig. 3) and there are no sharp non-equatorial peaks, bearing strong resemblance to the XRD of homo-polyacrylonitrile. The primary reflection (10) has a $d$-spacing of approximately 5.3 Å, and the weaker (11) reflection is at approximately 3.05 Å. Although, there are slight variations in the lattice parameter as a function of comonomer ratio and drawing condition, the ratio of the $d$-spacing of the two peaks remains $\sqrt{3}:1$ within an experimental accuracy, indicating hexagonal packing [8,9]. The diameter of the chain is: $(2/\sqrt{3})d_{(10)} = 6.1\,\text{Å}$. The lack of a meridional reflection indicates the lack of regularity along the chain, as expected from the 2D nature of the "crystalline" phase. Our results indicate that oriented copolymer fibers do not exhibit a significant amount of an amorphous phase [8,14].

Two important morphological features can be determined from the sharpness of the reflections. First, scanning the peak along the equatorial (Fig. 3b), the width of the peak measures the coherence length [26]. The coherence length depends strongly on the comonomer composition and more weakly on thermal annealing (which was accomplished during fiber production by passing the fibers over heated rolls) and/or the degree of fiber orientation. Values of the coherence length range from 40 Å for poorly oriented material containing 25% comonomer, to 145 Å for a more highly oriented fiber containing only 15% comonomer. The effect of fiber orientation is illustrated by the comparison of two fibers, designated **a** and **b**, of identical composition and spun under identical conditions, except that fiber **b** was also post drawn with an extension ratio of 2.5. The coherence length of the more highly oriented fiber **b** is 90 Å, while that of the more weakly oriented fiber **a** is 70 Å.

Second, azimuthal scans of the intensity of the (10)

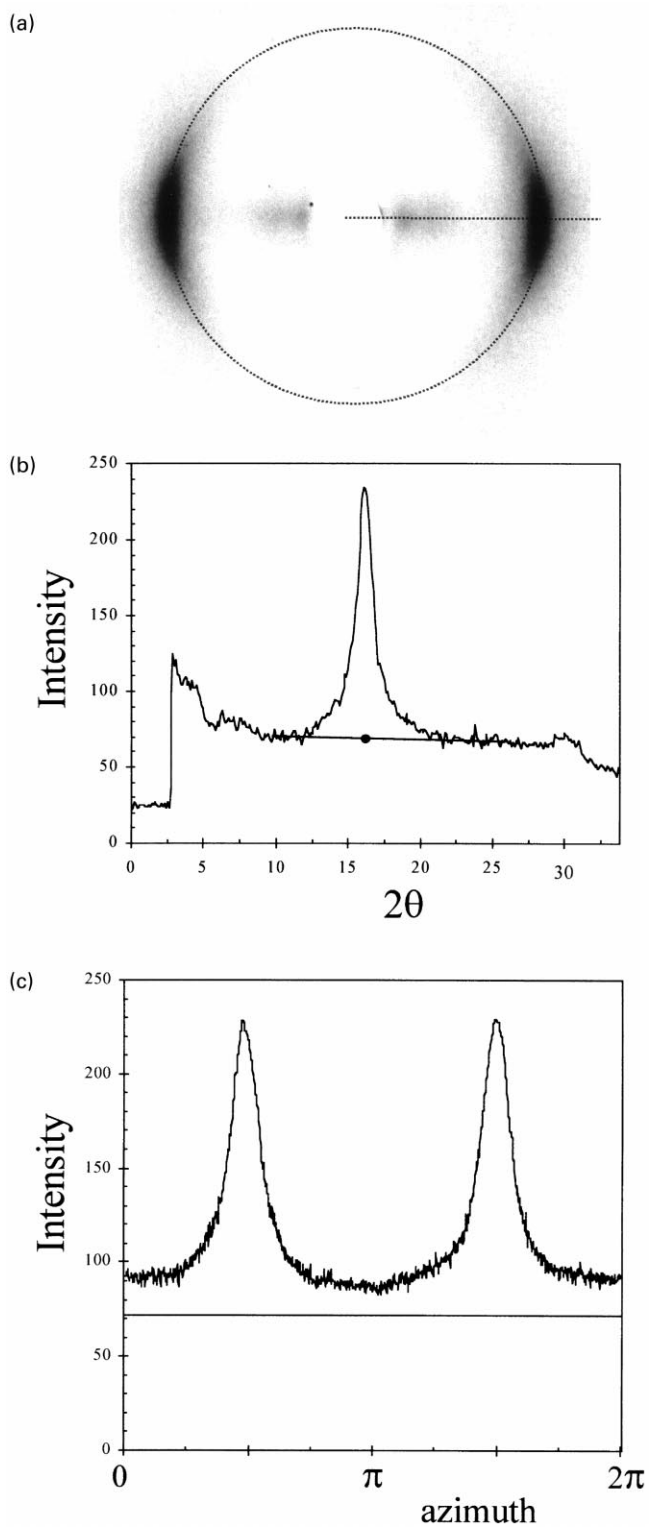


Fig. 3. (a) X-ray fiber diffraction pattern recorded from fiber **b**. The horizontal and circular dashed lines represent equatorial and azimuthal scans, respectively. (b) Equatorial scan of the diffraction pattern from fiber **c**. The dot illustrates the background intensity for the (10) peak. (c) Azimuthal scan of the diffraction pattern obtained from fiber **c**. The horizontal line represents the background intensity, which was determined from the equatorial scan and is subtracted before the application of Eq. (1). Because of the relatively poor orientation of this fiber in comparison to fiber **b**, the intensity of the (10) reflection is above the background level at all azimuthal angles.

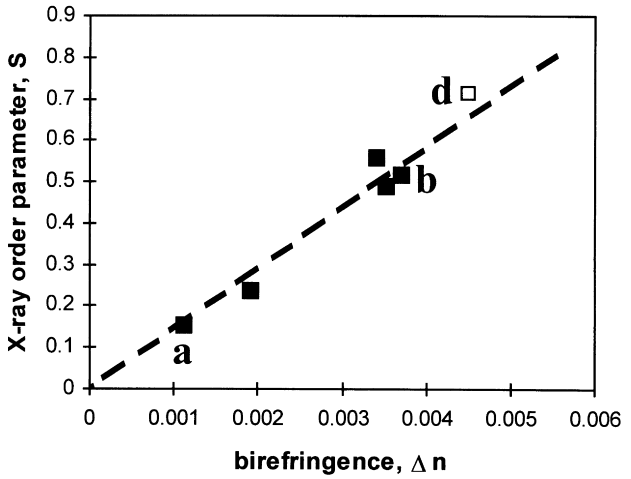


Fig. 4. Birefringence and X-ray order parameter of several fibers. Data points representing fibers **a** and **b** are labeled. Filled and open squares represent melt-spun AMLON® and solution-spun commercial fibers, respectively.

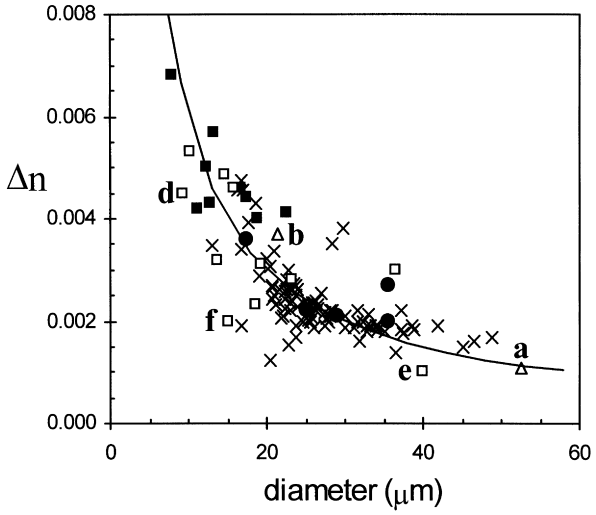


Fig. 5. Birefringence versus fiber diameter. Data points representing fibers **a**, **b**, **d**, **e** and **f** are labeled; refer to text for details. The filled symbols represent AMLON® melt-spun fibers that were processed at similar conditions, with the exception that the filled squares represent those fibers that were post-drawn 1.5 times. Open squares represent commercial solution-spun fibers. × symbols represent various other AMLON® fibers. Data points **a** and **b** are represented by triangles. The curve represents constant retardation.

reflection (Fig. 3c) were used to measure the degree of molecular orientation in the fiber, through the application of Eq. (2). A linear relationship between the orientational order parameter from XRD and the birefringence was observed (Fig. 4). Extrapolating the line to the unit order parameter, the maximum birefringence of these copolymers can be estimated to be: $\Delta n_{max} = 0.007$, which is weak in comparison to poly(ethylene terephthalate), for example. A relatively small value is to be expected, because the highly polarizable CN groups are oriented nearly perpendicular to the backbone direction, so that the side groups and the backbone nearly compensate one another. For polyacrylonitrile fibers having very little comonomer (approximately 1 wt.% [29]), the birefringence of highly aligned fibers is small and negative, i.e. $\Delta n = -0.004$ [29,30]. With larger fraction of comonomer, the birefringence of aligned fibers is positive, but $\Delta n_{max}$ remains small. Therefore, the slope of the linear relationship between birefringence and orientational order parameter (Fig. 4) depends on composition. The orientational order parameter (measured by XRD) and the birefringence of a commercial solution spun fiber (**d**) was also investigated. The point *d* lies near the linear relationship established for the melt-spun AMLON® fibers, suggesting its similar composition.

The IR measurement of the order parameter is in qualitative agreement with the X-ray analysis. The dichroic ratio of the nitrile stretching band (2244 $cm^{-1}$) was measured for different fibers, one weakly and the other highly oriented (fibers **a** and **b**, respectively). Assuming the angle between the transition moment and the polymer chain direction to be 70° [15,31,32], one calculates the order parameter of these fibers to be 0.14 and 0.48, respectively. These values agree closely with those obtained through XRD analysis: 0.15 and 0.52, respectively. Assuming a slightly smaller angle between the transition moment and the polymer chain (69°), even better agreement is achieved. The close agreement between XRD, IR dichroism and birefringence likely stems from the lack of a significant amount of isotropic phase.

The birefringence of many different fibers was measured to compare the effect of different spinning conditions. In general, we find an inverse correlation between the fiber diameter and the birefringence (Fig. 5). That is, those processes that produce fine denier fibers also generally produce a high orientation. However, this represents only a general trend, and significant differences in retardation were measured for different fibers: measurements ranged between 25 and 113 nm. Commercial solution-spun fibers fall along the same general trend, exhibiting intermediate properties, e.g. fiber **d**. In some cases, the draw ratio of these fibers is very high. Points labeled **e** and **f**, represent commercial fibers analyzed by Rizzo et al. [33] which were drawn two and 14 times, respectively. Their relatively low $\Delta n$ may indicate that either the fibers have poorer orientation or they are relatively richer in acrylonitrile, thus having a smaller $\lambda n_{max}$. Unfortunately, the uncertainty remains, because neither the composition nor an independent measure of order parameter was reported in that study.

As illustrated in Fig. 5, post-drawn fibers have among the highest orientation. Indeed, cold drawing or post-drawing has the most dramatic effect on molecular orientation [15]. Filled circles in Fig. 5 represent as-spun fibers that were spun under the same conditions as the filled squares, the latter representing fibers that were post-drawn. Significant effects of post-drawing are observed even for small draw ratio, i.e. $\lambda = 1.5$. It should be also noted that the effect of

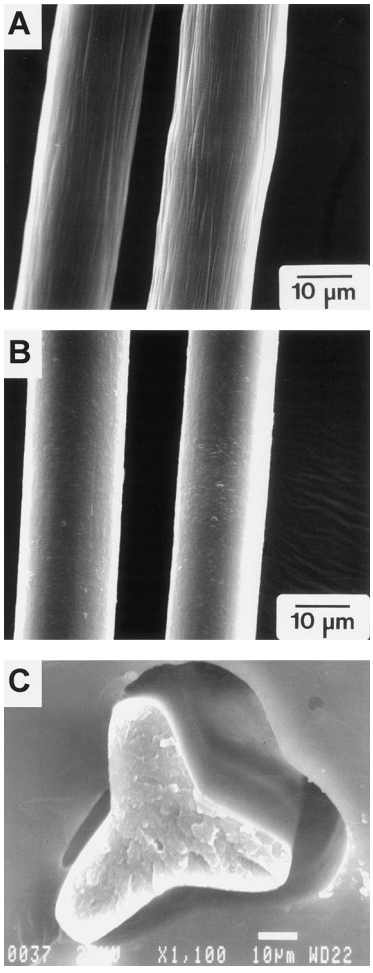


Fig. 6. SEM of: (a) commercial solution-spun fiber; (b) AMLON® melt-spun fiber; (c) AMLON® trilobal fiber. The embedding material surrounding the fiber has pulled away, causing the shadow-like appearance.

post-drawing saturates at small values of $\lambda \sim 2$. This is consistent with the fact that the chains are partially aligned before post-drawing and the entanglement density in the solvent free state (determined from rheological analysis) is relatively high. Additional drawing does not cause failure, but neither does it increase orientation.

Initial drawing conditions are less significant because the entanglements are sufficiently short lived at elevated temperature that a high degree of orientation cannot be achieved. Since the degree of molecular orientation that can be achieved is a function of the relative deformation and molecular relaxation rates, a greater degree of orientation is anticipated if the spinning is done at a higher speed, lower temperature or with a higher molecular weight polymer. Indeed, increasing the molecular weight provided a substantial improvement in orientation under spinning conditions (constant temperature and die size) that produced a 15 denier as-spun fiber from a moderate molecular weight material and a 20 denier as-spun fiber from a high molecular weight material. In spite of the fact that the higher molecular weight material was drawn less (larger denier), the orientational order parameter (X-ray) was 0.16 and 0.4 for the moderate and high molecular weight materials, respectively.

Heat setting or annealing (the process of passing the fiber over heated rolls after post-drawing) does not increase molecular orientation. Instead, it increases "crystal" size. For a variety of fibers that were spun under different conditions, heat setting at approximately 150°C produced a 30–40% increase in crystal size.

AMLON® melt-spun fibers differ from solution spun fibers in terms of their surface morphology. While commercial solution-spun fibers have rough grooves and an irregular shape [34], the melt-spun fibers are relatively smooth and cylindrical (Fig. 6). The cross-section of the fiber can be adjusted easily by die design (Fig. 6c).

## 4. Conclusions

The image intensity profile measured from an aligned fiber under cross-polars has been fitted accurately. The birefringence of many melt-spun AMLON® and other commercial solution-spun fibers is measured. The birefringence correlates well with the orientational order parameter measured by XRD. The orientation of the AMLON® fibers is as good or better than that of commercial solution-spun fibers. Post-drawing has a dramatic effect on molecular orientation. Heat setting increases crystal size without sacrificing orientation. Higher molecular weight increases orientation.

## Acknowledgements

The authors gratefully acknowledge the financial support of BP Amoco Chemicals. The assistance of Prof. J.L. Koenig's laboratory for the infrared dichroism experiments is also gratefully acknowledged.

## References

[1] Kamide K, Yamazaki H, Okajima K, Hikichi K. Polym J 1985;17:1233.
[2] Clarke AJ, Bailey JE. Nature 1973;243:146.
[3] Hinrichsen GJ. Appl Polym Sci 1973;17:330.
[4] Sen K, Bahrami SH, Bajaj P. J Macromol Sci, Rev Macromol Chem Phys 1996;C36:1.
[5] Keller A, Machin MJ. J Macromol Sci (Phys) 1967;B1:41.
[6] Spruiell JE, White JL. In: White JL, editor. Applied polymer symposium, 27. London: Wiley, 1975. p. 121.
[7] Frushour BG, Knorr RS. In: Lewin M, Pearce EM, editors. Handbook of fiber science and technology, Fiber chemistry, 4. New York: Marcel Dekker, 1985. p. 212.
[8] Bohn CR, Scharfgen JR, Statton WO. J Polym Sci 1961;55:531.
[9] Allen RA, Ward IM, Bashir Z. Polymer 1994;35:4035.
[10] Allen RA, Ward IM, Bashir Z. Polymer 1994;35:2063.
[11] Andrews FD, Miyachi K, Doshi RS. Polym Prepr 1972;13:1168.
[12] Gupta AK, Singhal RP. J Polym Sci Polym Phys 1983;21:2243.
[13] Bashir Z, Atureliya SK, Church SP. J Mater Sci 1993;28:2721.

[14] Liu XD, Ruland W. Macromolecules 1993;26:3030.
[15] Bashir Z, Tipping AR, Church SP. Polym Int 1994;33:9.
[16] Chen JY, Tucker PA, Cuculo JA. J Appl Polym Sci 1997;66:2441.
[17] Huang B, Tucker PA, Cuculo JA. Polymer 1997;38:1101.
[18] Wu G, Jiang JD, Tucker PA, Cuculo JA. J Polym Sci, Polym Phys 1996;34:2035.
[19] Wu G, Tucker PA, Cuculo JA. Polymer 1997;38:1091.
[20] Hermans PH. Contribution to the physics of cellulose fibres: a study in sorption, density, refractive power and orientation, Amsterdam: Elsevier, 1946.
[21] Huijts RA, Peters SM. Polymer 1994;35:3119.
[22] Kuhn W, Grun O. Kolloid Z 1942;101:248.
[23] Treloar LRG. The physics of rubber elasticity, 2nd. Oxford, UK: Oxford University Press, 1958.
[24] Davidson JA, Butler RS. Particle and Particle Systems Characterization 1992;9:213.
[25] International tables for X-ray crystallography, Dordrecht, Netherlands: Kluwer Academic, 1989.
[26] Alexander LE. X-ray diffraction methods in polymer science, New York: Wiley-Interscience, 1969.
[27] Mitchell GR, Windle AH. In: Bassett DC, editor. Developments in crystalline polymers—2, London: Elsevier Applied Science, 1988. p. 115.
[28] Fraser RDB. J Chem Phys 1956;24:89.
[29] Kakida H, Tashiro K. Polym J 1998;30:474.
[30] Heyn ANJ. Text Res J 1952;22:513.
[31] Zbinden R. Infrared spectroscopy of high polymers, New York: Academic Press, 1964.
[32] Siesler HW. Makromol Chem 1975;176:2451.
[33] Rizzo P, Guerra G, Auriemma F. Macromolecules 1996;29:1830.
[34] Masson JC. In: Masson JC, editor. Acrylic fiber technology and applications, New York: Marcel Dekker, 1995. p. 388.